Q. J. R. Meteorol. Soc. (2001), **00**, pp. 1–19

Impact of new measurements of oxygen collision-induced absorption on estimates of short-wave atmospheric absorption

By J. C. S. CHAGAS[1]*, D. A. NEWNHAM[2], K. M. SMITH[2] and K. P. SHINE[1]
[1]*Department of Meteorology, University of Reading, UK*
[2]*Space Science and Technology Department, Rutherford Appleton Laboratory, UK*

(Received 1 January 2001; revised 31 December 2001)

SUMMARY

A new set of laboratory measurements of the 1.06-μm and 1.27-μm collision-induced bands of gaseous oxygen is presented. Absorption by pure oxygen and mixtures of oxygen with nitrogen and argon was observed using a Fourier transform spectrometer for temperatures between 230 and 295 K and pressures between 1 and 5 bar. Binary cross-sections derived from the measurements were used to estimate the impacts on estimates of clear-sky climatological absorption of solar irradiance. Monthly climatological atmospheric profiles averaged over 10-degree-latitude belts were used to study the temporal and annual variation of the impacts. Global and annual mean clear sky extra-absorption was 0.58 Wm^{-2} (about 1% of the absorption by water vapour and ozone), 0.42 Wm^{-2} due to the 1.27-μm band and 0.16 Wm^{-2} due to the 1.06-μm band. If estimates for other oxygen collision-induced bands taken from previous studies are added, an overall impact of about 1 Wm^{-2} results.

KEYWORDS: Short-wave absorption Collision-induced absorption Oxygen

1. INTRODUCTION

There remains a considerable debate over the amount of solar radiation absorbed by the atmosphere in both clear and cloudy skies (*e.g.* Arking 1999a, 1999b, Halthore and Schwartz 2000, Zender *et al.* 1997, Wild and Ohmura 1999). For clear skies, there is a divergence of opinion as to whether observations are in agreement with models. Mlawer *et al.* (2000) and Brown *et al.* (1999a, 1999b) consider that there is no evidence for any disagreement, whilst Halthore and Schwartz (2000) find that models underestimate the absorption by 4% and Wild and Ohmura (1999) find a model underestimate of about 10%. There are several possible causes of such a discrepancy, if it exists. Some studies regard water vapour as the major cause of the discrepancy whilst acknowledging the possible importance of aerosols (Arking 1999a, 1999b). Updates to water vapour spectral databases can cause an increased absorption of around 1% (Chagas *et al.* 2001, Zhong *et al.* 2001) as can absorption by the water vapour dimer (Vaida *et al.* 2001). The possibility of some missed gaseous absorption process at visible wavelengths was also pointed out (Kato *et al.* 1997) and evidence of the importance of absorbing aerosols has been presented (Cusack *et al.* 1998, Wild 1999). The present paper investigates the possible impact of collision-induced oxygen bands on estimates of short-wave atmospheric absorption.

Absorption of solar radiation by oxygen has been included in recent comprehensive radiative transfer schemes inside GCMs. This is usually done by using line parameters from spectroscopic databases, which refer to transitions allowed by spectroscopic selection rules. However, otherwise forbidden transitions can be induced by collisions between molecules. In contrast to the absorption lines of the free molecule, these collisional bands appear as unstructured absorption continua. As cross-section data for these bands are usually limited in spectroscopic databases, their effects have generally not been adequately accounted for in current GCMs.

In the case of oxygen, the selection rules for some electric dipole forbidden transitions in one or both molecules are relaxed during collisions and absorption can

* Corresponding author: Centro de Previsão de Tempo e Estudos Climáticos CPTEC-INPE, Rodovia Pres. Dutra km 40, 12630-000 Cachoeira Paulista SP, Brazil; email: julio@cptec.inpe.br

occur. Those transitions can also be induced by collisions between oxygen and different molecules. This phenomenon has been observed for about a century (see *e.g.* Solomon *et al.* 1998 and references therein) and its possible contribution to the anomalous short-wave absorption problem has been the focus of several recent studies (*e.g.* Pfeilsticker *et al.* 1997, Mlawer *et al.* 1998, Solomon *et al.* 1998, Zender 1999).

Greenblatt *et al.* (1990) carried out laboratory measurements of the cross-sections over the visible/near-ultraviolet (visible for short) and 1.06-μm bands, which form the basis for some of the subsequent estimates of the global effect of the collision-induced short-wave absorption by oxygen summarised in Table 1. Pfeilsticker *et al.* (1997) combined these measurements with atmospheric observations to produce their global estimates.

TABLE 1. GLOBALLY AVERAGED SHORT-WAVE ABSORPTION BY OXYGEN COLLISION COMPLEXES FROM DIFFERENT STUDIES.

Complex:		O_2-O_2			O_2-N_2	Total
Band:	Vis	1.06-μm	1.27-μm	1.58-μm	1.27-μm	
Pfeilsticker *et al.* (1997)		0.53	–	–	–	0.53 (c)
		0.57	–	–	–	0.57 (a)
Mlawer *et al.* (1998)	–	0.10	0.29	0.03	–	0.42 $\rightarrow$ 0.84 (c)
Solomon *et al.* (1998)	0.42	0.19	0.19–0.30	–	0.07–0.31	0.87–1.22 (c)
	0.45	0.20	0.20–0.32	–	0.08–0.34	0.93–1.31 (a)
Zender (1999)		0.78		–	0.17	0.94 (c)
		0.78		–	0.15	0.93 (a)

All values in Wm^{-2}. Vis: visible/near-ultraviolet band; c: clear sky; a: all sky. Total of Mlawer *et al.* (0.84) includes 0.42 for the visible band taken from Solomon *et al.*

Mlawer *et al.* (1998) used high-resolution atmospheric observations of the three main collision-induced bands of the infrared system to evaluate their combined global impact on short-wave absorption. Solomon *et al.* (1998) used the Greenblatt *et al.* (1990) cross-sections for the visible and 1.06-μm collision-induced bands. For the 1.27-μm collision-induced band, they stretched the 1.06-μm band shape in order to fit relationships between the integrated intensity of the two bands taken from older low resolution measurements (Dianov-Klokov 1964, McKellar *et al.* 1972). They also used previous estimates of the efficiency of nitrogen as a collision partner if compared with oxygen itself to estimate the additional absorption by oxygen-nitrogen collisions (Ketelaar 1955, Cho *et al.* 1963, Badger *et al.* 1965). As a consequence of using estimates from different studies, their 1.27-μm-band and total results are presented in Table 1 as ranges of variation rather than specific values. They stressed the need for "modern" laboratory observations of the 1.27-μm collision continuum.

All those studies took estimates for a particular atmospheric profile and extrapolated them to mean global conditions, a procedure that attaches some uncertainty to their figures. Pfeilsticker *et al.* (1997) made some assumptions and estimated a global mean of 0.57 Wm^{-2} for the oxygen collision-induced absorption, which is about 42% of their estimates of 1.35 Wm^{-2} for mid-latitude summer atmosphere, overhead Sun, clear-sky absorption. Solomon *et al.* (1998) adopted the same ratio to produce global estimates from mid-latitude summer, overhead Sun absorption. But the differences between global estimates (especially between figures from Mlawer *et al.* 1998 and Solomon *et al.* 1998) are mainly associated with differences in the cross-sections.

Zender (1999) used a GCM to obtain a temporal and spatial distribution of the effect of oxygen collision pairs on atmospheric absorption using Solomon *et al.*'s (1998) cross-sections. He considered the cross-sections constant with temperature and made particular choices for the scaling factor between integrated intensities of the 1.06-μm

and 1.27-μm bands and for the efficiency of nitrogen as a collision partner from the range of values summarised by Solomon *et al.* (1998). His global results (Table 1) are a true global mean derived using a GCM climatology but they share the main weakness of the other studies (except perhaps Mlawer *et al.* 1998), the rather crude estimates of the cross-sections for the 1.27-μm band. Recent high-resolution laboratory measurements of the 1.27-μm continuum are reported by Maté *et al.* (1999) and Smith and Newnham (1999, 2000), who also report measurements of the 1.06-μm continuum. Smith and Newnham's (1999, 2000) measurements were all made at about 1 bar pressure.

In order to confidently extrapolate laboratory cross-sections to atmospheric conditions (pressures below 1000 hPa) and better describe the collision-induced bands, this paper presents a new set of measurements carried out at the Molecular Spectroscopy Facility (MSF) of the Rutherford Appleton Laboratory (RAL) using a Fourier transform spectrometer (FTS). They included pure oxygen and mixtures of oxygen with nitrogen and argon for temperatures between 230 and 295 K and pressures between 1 and 5 bar. An absorber pathlength of about 13 m was used. Our aim here is to describe these new measurements and their use to estimate the impact of the oxygen collision-induced bands on the atmospheric short-wave absorption. Section 2 describes the laboratory measurements and the process used to obtain cross-sections from the recorded spectra. Also presented is an error analysis of the resulting cross-sections and comparisons with previous measurements. Section 3 deals with the use of the derived cross-sections in atmospheric radiative transfer calculations. Calculations for a particular atmospheric profile are presented and followed by a discussion of climatological estimates for selected months over latitude belts along with global averages. The main conclusions are presented in Section 4.

2. LABORATORY MEASUREMENTS

(*a*) *Description of the experiments*

Experimental details of the measurements carried out at the MSF/RAL are described by Newnham and Ballard (1998) and Smith and Newnham (2000) and can be summarised as follows:

Spectrometer: Bruker IFS 120HR Fourier transform spectrometer.

Source: 150 W quartz-tungsten-halogen (Osram Type HLX61640).

Beam-splitter: silica-coated calcium fluoride (near-infrared).

Spectral resolution: defined as 0.9/MOPD, where MOPD is the maximum optical path difference between the fixed and moving mirror of the spectrometer's interferometer. Apodisation (Norton-Beer, Strong for resolution = 0.05 cm^{-1} and Blackman-Harris, 3-term at lower resolutions) has been applied to all sample and background spectra.

Gas cell: RAL short pathlength absorption cell (SPAC). The optical pathlength is given by the expression $((2n + 2) \times R) + d$ where $n = 1, 3, 5, ...$ is the number of images on the field mirror and R is the radius-of-curvature of the spherical "White" optics mirrors, *i. e.*, 0.400 m. The distance d is the absorber pathlength between the optical windows of the SPAC and the front surface of the field mirror, and is measured to be 0.138($\pm$0.001) m. For this work the SPAC output focusing mirror was adjusted to produce 15 images (n = 15) on the field mirror and a total absorber pathlength of 12.938($\pm$0.033) m.

Sample handling: clean high-pressure stainless vacuum lines.

Temperature sensors: six 10 kohm thermistors in thermal contact with the gas samples.

Pressure sensors: calibrated 1000 torr and 5 bar full-scale absolute Baratron capacitance gauges (MKS Types 750B and 390).

Twenty nine experiments were carried out (Table 2).

TABLE 2. SAMPLE DESCRIPTION, TEMPERATURE AND PRESSURE FOR THE DIFFERENT MEASUREMENTS OF OXYGEN CROSS-SECTIONS.

Experiment no.	Sample	Temperature (K)	Pressure (hPa)
1	21% O_2 in N_2	294.4	502.4
2	21% O_2 in N_2	294.5	1005.6
3	21% O_2 in N_2	294.6	1518.1
4	21% O_2 in N_2	294.7	2510.3
5	21% O_2 in N_2	295.0	4982.0
6	21% O_2 in N_2	261.8	1517.2
7	21% O_2 in N_2	261.3	2513.2
8	21% O_2 in N_2	261.0	3500.9
9	21% O_2 in N_2	260.7	5005.4
10	21% O_2 in N_2	233.8	2483.2
11	21% O_2 in N_2	231.5	3501.5
12	21% O_2 in N_2	230.5	4979.7
13	21% O_2 in N_2	229.4	1507.8
14	21% O_2 in Ar	278.7	1007.7
15	21% O_2 in Ar	280.1	1509.9
16	21% O_2 in Ar	281.8	2513.7
17	21% O_2 in Ar	283.6	3507.7
18	21% O_2 in Ar	284.7	5006.3
19	21% O_2 in Ar	285.2	2517.3
20	O_2	293.1	1011.3
21	O_2	293.3	1508.5
22	O_2	293.5	2517.0
23	O_2	293.7	3518.7
24	O_2	293.9	4997.7
25	21% O_2 in N_2	294.3	3508.3
26	O_2	230.3	1006.7
27	O_2	228.0	2497.9
28	O_2	226.5	3490.5
29	O_2	225.8	4972.1

(*b*) *Data conversion*

The spectra were originally recorded at an instrument resolution of 0.05 cm^{-1} and subsequently transformed to produce higher signal-to-noise spectra at a resolution of 0.5 cm^{-1}. For the work described here the 0.5-cm^{-1}-resolution sample spectra were used and the average of two background spectra at the same resolution (one recorded before and another after each day's measurements) was used as the background for the day. The following, which closely follows Smith and Newnham (2000), describes the main steps of the conversion of raw spectra into binary cross-sections.

The concentration c (mol cm^{-3}) of O_2 molecules in the gas sample is given by

$$c = \frac{pf}{RT}, \tag{1}$$

where p is the total gas pressure (Pa), f is the O_2 volume fraction, R is the gas constant (JK^{-1}) and T is the gas temperature (K). It is assumed that the gas mixture behaves as an ideal gas and that there is little contribution to the pressure from O_4 dimers. The optical transmittance $\tau_c(\tilde{\nu}, T, p)$ at wavenumber $\tilde{\nu}$ (cm^{-1}) of sample concentration c at temperature T and pressure p was determined as the ratio of the sample intensity $I(\tilde{\nu}, T, p)$ to the background spectrum intensity $I_0(\tilde{\nu}, T, p)$,

$$\tau_c(\tilde{\nu}, T, p) = \frac{I(\tilde{\nu}, T, p)}{I_0(\tilde{\nu}, T, p)}. \tag{2}$$

The Napierian absorbance (or optical depth) $A(\tilde{\nu}, T, p)$ is given by

$$A(\tilde{\nu}, T, p) = -\ln \tau_c(\tilde{\nu}, T, p). \tag{3}$$

A relevant parameter is the number N_p of molecular pairs involving oxygen molecules in a unit volume of gas (molecule^{2}cm^{-6}), which is given by Vigasin (1996):

$$N_p = \frac{N_A\, c(N_A\, c - 1)}{2} \approx \frac{(N_A\, c)^2}{2}, \tag{4}$$

where N_A is the Avogadro constant.

Also relevant (in fact, the parameter to be used as input in the radiative transfer calculations) is the binary absorption cross-section (cm^{5}molecule^{-2}) defined as

$$\sigma_{bin}(\tilde{\nu}, T, p) = \frac{A(\tilde{\nu}, T, p)}{2N_p l}\ , \tag{5}$$

where l is the optical pathlength (m) through the absorber gas (O_2) of molecular pair number density N_p. The binary absorption cross-section is preferred over the monomer absorption cross-section as the latter would be heavily pressure dependent as the number of oxygen pairs varies with pressure via Eqs (1) and (4).

The procedures used here to convert the raw spectra to binary cross-sections, which includes careful baseline corrections for the spectra, were described in detail by Newnham and Ballard (1998) and Smith and Newnham (2000).

For the 1.27-μm band there is a line-structured absorption due to the magnetic dipole transition superimposed on the continuum due to collision processes. To obtain the continuum cross-sections it is necessary to remove the line contribution. The Reference Forward Model (RFM) of the University of Oxford (Dudhia 1997) was used to generate, for the conditions of each measurement, synthetic binary cross-section spectra for the oxygen lines based on HITRAN 1996 (Rothman *et al.* 1998), which were subsequently subtracted from the measured spectra. The result of that operation was taken to be the continuum due to collisions. For low pressure (1.5 bar or less) the resulting data were discarded because of the large baseline noise. For higher pressure data, it was possible to remove the dominant features associated with the line absorption. Note that this procedure, which is illustrated in Figure 1, differs from that adopted by Smith and Newnham (2000), where a more subjective method was adopted to separate lines and continua.

For the 1.06-μm band the line-structured absorption is very weak (see Solomon *et al.* 1998) and falls within the random noise of the measurements and so the measured cross-sections were taken as due to the continuum. However, the main problem with the measured spectra for this band is the low information-to-noise ratio. Figure 2 shows the spectra for measurements with oxygen-nitrogen mixtures at about 260 K and different pressures. Even for the measurement at 5.0 bar the fluctuations are so large that they compromise the usefulness of the data. The spectra obtained with pure oxygen samples exhibit much less noise (Figure 3).

For each measurement, the integrated binary absorption intensity (cm^{4}molecule^{-2}) was calculated separately for each continuum band using

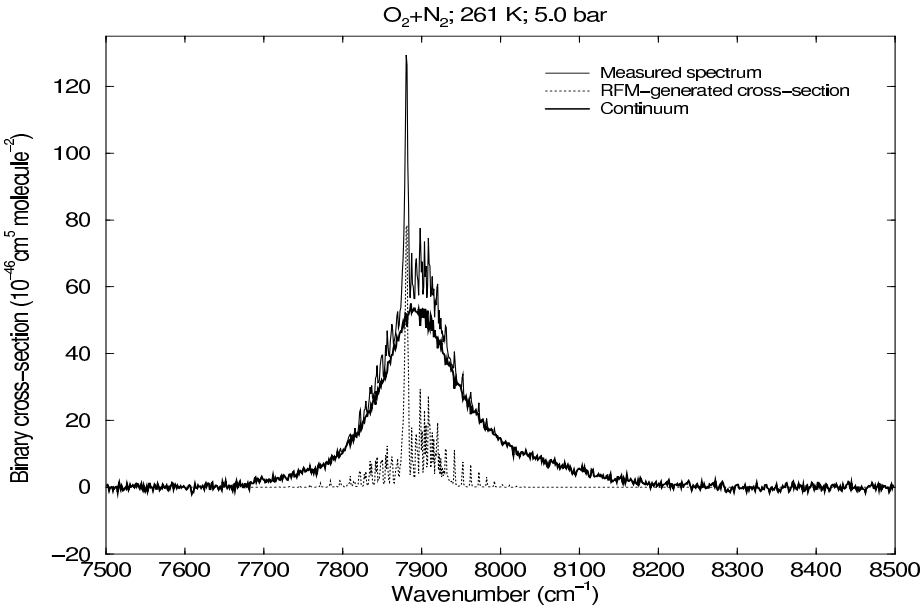

Figure 1. Binary cross-section for the absorption continuum in the 1.27-μm band of oxygen obtained by subtracting RFM-generated line structured absorption from measurements for a 21% mixture of oxygen in nitrogen at 261 K and 5.0 bar (experiment 9 in Table 2).

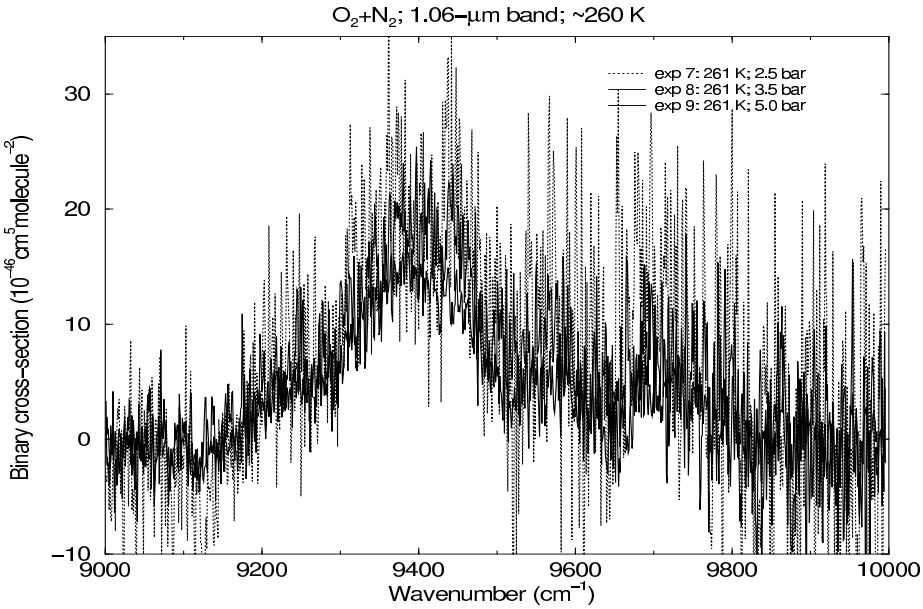

Figure 2. Binary cross-sections for the absorption continuum in the 1.06-μm band of oxygen for a 21% mixture of oxygen in nitrogen at 261 K and 2.5, 3.5 and 5.0 bar (experiments 7, 8 and 9 in Table 2).

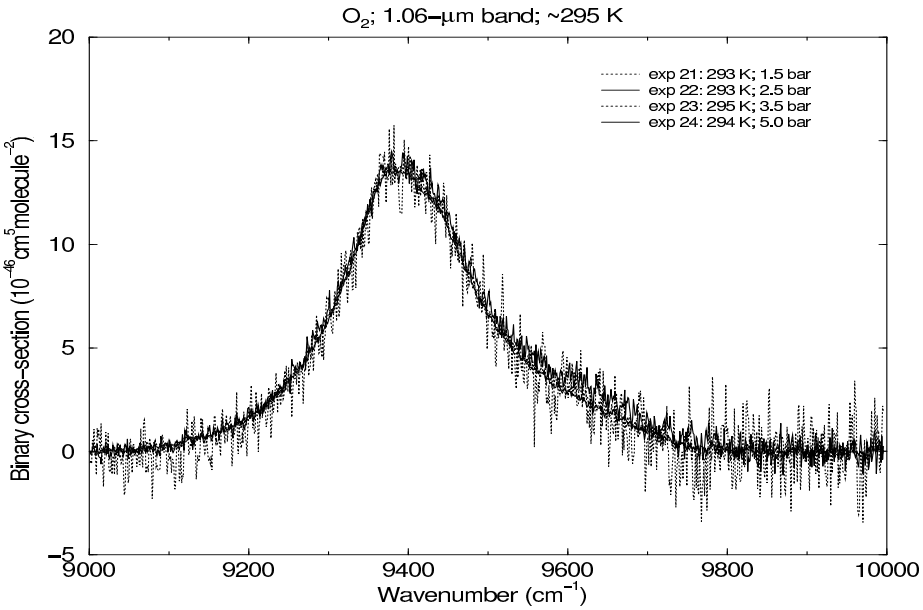

Figure 3. Binary cross-sections for the absorption continuum in the 1.06-μm band of oxygen for pure oxygen samples at about 295 K and 1.5, 2.5, 3.5 and 5.0 bar (experiments 21, 22, 23 and 24 in Table 2).

$$S_{bin}(T,p) = \int_{\tilde{\nu}_1}^{\tilde{\nu}_2} \sigma_{bin}(\tilde{\nu},T,p)d\tilde{\nu}, \tag{6}$$

where the limits of integration were chosen to include the whole of the absorbing region and avoid regions contaminated with a small absorption by water vapour present in the spectra. For the 1.27-μm band the limits were 7500 and 8500 cm^{-1} and, for the 1.06-μm band, 9000 and 10,000 cm^{-1}.

(*c*) *Error analysis*

The error analysis used for the resulting binary cross-section values is close to that described in detail by Newnham and Ballard (1998) and Smith and Newnham (2000). From Eqs (5) and (4), the standard deviation (in $cm^5 molecule^{-2}$) associated with each value of the binary cross-section is given by:

$$s_{\sigma_{bin}}(\tilde{\nu},T,p) = \sigma_{bin}(\tilde{\nu},T,p)\sqrt{\left[\frac{\sigma_A(\tilde{\nu},T,p)}{A(\tilde{\nu},T,p)}\right]^2 + 2\left(\frac{\sigma_c}{c}\right)^2 + \left(\frac{\sigma_l}{l}\right)^2}, \tag{7}$$

where $\tilde{\nu}$ is the wavenumber (cm^{-1}), T is the temperature (K), $A(\tilde{\nu},T,p)$ is the absorbance, $\sigma_A(\tilde{\nu},T,p)$ is the standard deviation associated with the absorbance, c is the oxygen concentration and σ_c the standard deviation associated with it, l is the optical pathlength (m) and σ_l its associated standard deviation.

The optical pathlength l and its associated standard deviation σ_l for all measurements are respectively 12.938 m and 0.033 m. The standard deviation in absorbance $\sigma_A(\tilde{\nu},T,p)$ is taken into account during the process of data reduction and the root

mean square error associated with the baseline noise in the spectrum was included in its estimate. The standard deviation in oxygen concentration is given by

$$\sigma_c = c\sqrt{\left(\frac{\sigma_p}{p}\right)^2 + \left(\frac{\sigma_f}{f}\right)^2 + \left(\frac{\sigma_T}{T}\right)^2}, \tag{8}$$

where σ_p, σ_f and σ_T are the standard deviations associated with pressure, oxygen fraction and temperature respectively. Each measurement lasted typically about 30-40 minutes and the temperature (6 sensors) and pressure (1 or 2 gauges) were recorded every 5 minutes. Temperature and pressure values in Table 2 are the average of all readings during each experiment. Temperature and pressure uncertainties used in Eq (8) were a combination of the standard deviation of the set of readings with the stated accuracy of the sensors. The 5 bar full-scale Baratron (MKS 750B) and the 1000 torr full-scale absolute Baratron (MKS 390) capacitance gauges have stated accuracies of 1% and 0.08% of reading respectively. The manufacturer's uncertainties of the thermistors are 0.2 K for the experiments at temperatures above 230 K and 0.45 K at 230 K.

The supplier-stated gas purity was $99.99 \pm 0.01\%$ for pure oxygen and $21.0 \pm 0.5\%$ oxygen and $79.0 \pm 0.5\%$ nitrogen for the oxygen-nitrogen mixtures. The uncertainty associated with the gas fraction for the oxygen-argon mixtures depends on the purity of the gases used for the mixture, on uncertainties in the measured pressure and temperature after filling the cell with the first component, in the measured temperature during measurements and on how well mixed the gases are. A worst-case uncertainty in oxygen/argon mixing ratio of 5% was used here.

The uncertainty attached to the integrated binary absorption intensity (Eq (6)) was calculated as

$$\sigma_{S_{bin}} = \int_{\tilde{\nu}_1}^{\tilde{\nu}_2} S_{\sigma_{bin}}(\tilde{\nu}, T, p) d\tilde{\nu}. \tag{9}$$

(*d*) *Temperature and pressure dependency of integrated intensity*

Previous studies mentioned in Section 1 needed a value of the effectivity of nitrogen as a collision partner if compared to oxygen because they estimated $O_2 - N_2$ absorption from $O_2 - O_2$ cross-sections available at that time. But here cross-sections for mixtures of 21% oxygen in nitrogen (which include $O_2 - O_2$ and $O_2 - N_2$ absorption) were available and could be taken directly as representative of atmospheric air without the need for estimating such an efficiency factor. So, cross-sections from experiments 1 to 13 and 25 (Table 2) were initially chosen to form the basis to the input for radiative transfer calculations which would include some temperature dependence of cross-sections.

However, inspection of curves of cross-sections against wavenumber for those measurements revealed that some of them were too noisy to be useful for that purpose. This was quantitatively confirmed by inspecting the integrated binary absorption intensities and especially their uncertainties as shown in Table 3. The much larger uncertainty present in the 1.06-μm figures are mainly due to larger uncertainties in the baseline caused by the lower detector response compared to that in the 1.27-μm region.

Some measurements were then discarded mainly because of massive uncertainty and nine were kept (those marked with $\surd$ in the table). They are experiments at temperatures near 230, 260, and 295 K, and at 2.5, 3.5, and 5.0 bar pressure for each of those temperatures. The integrated absorption intensities for those experiments are

TABLE 3. INTEGRATED BINARY ABSORPTION INTENSITY (S_{bin}) AND ITS STANDARD DEVIATION FOR THE 1.27-μm AND 1.06-μm CONTINUA MEASURED FOR OXYGEN-NITROGEN MIXTURES UNDER DIFFERENT CONDITIONS.

Experiment	T (K)	p (bar)	S_{bin}	$\sigma_{S_{bin}}$	S_{bin}	$\sigma_{S_{bin}}$	
			1.27-μm continuum		*1.06-μm continuum*		
1	295	0.5	47.69	94.84	25.83	281.67	
2	295	1.0	12.00	24.19	5.15	64.99	
3	295	1.5	6.48	10.90	5.66	28.84	
4	295	2.5	7.15	4.01	3.95	11.25	√
25	295	3.5	9.35	2.34	5.39	5.73	√
5	295	5.0	8.75	1.25	1.43	2.79	√
6	260	1.5	5.73	9.66	16.78	27.39	
7	260	2.5	6.74	3.27	6.51	10.08	√
8	260	3.5	7.79	1.78	5.48	5.35	√
9	260	5.0	8.04	1.00	3.68	2.51	√
13	230	1.5	27.76	8.01	2.42	26.82	
10	230	2.5	9.69	3.22	8.97	10.54	√
11	230	3.5	11.51	1.67	3.38	4.71	√
12	230	5.0	10.66	1.00	2.61	2.54	√

Units are 10^{-43}cm^{4}molecule^{-2}. Experiment numbers as described in Table 2. Temperature (T) and pressure (p) are approximate values of figures from Table 2. A √ shows which data were eventually used in the atmospheric radiative transfer calculations.

displayed in Figure 4 for the 1.27-μm band. The first column shows the integrated absorption intensity as a function of pressure for the different temperatures. Assuming that the continuum features are due to collision-pair absorption, the integrated binary intensities are expected to be independent of pressure and the evidence in the figures support this, if the uncertainties are taken into account.

The temperature dependence of the integrated absorption intensity is a matter of controversy (Greenblatt *et al.* 1998, Newnham and Ballard 1998, and Osterkamp *et al.* 1998). Again due to the uncertainty of the data presented here, it is still not possible to define the behaviour of the integrated intensity with temperature. So, it seems sensible to take the average of the nine measurements as the temperature and pressure independent value to be used in the radiative transfer calculations. For the 1.27-μm band the averaged integrated binary intensity is $8.85(\pm 2.17) \times 10^{-43}$cm^{4}molecule^{-2}. A similar analysis for the 1.06-μm band again showed no obvious pressure and temperature dependence but the derived integrated binary intensity $4.60(\pm 6.17) \times 10^{-43}$cm^{4}molecule^{-2} was too uncertain to be used. A more reliable estimate is derived using the pure oxygen observations reported in the next sub-section (see also Figure 3). Details on how the averaged cross-sections were used in the radiative transfer model will be presented below (Section 3).

(*e*) *Comparisons with previous studies*

Results from experiments with oxygen-nitrogen mixtures were chosen for the main analysis because the focus of the work was to estimate the climatological absorption due to oxygen collision pairs. However, the availability of different samples (oxygen-nitrogen, oxygen-argon, pure oxygen) at different pressures allows subsidiary observations on some related problems mentioned in the literature.

1 *1.06-μm collision-induced band*

For the 1.06-μm band there is apparently no effect of nitrogen or argon on the cross-sections, a fact observed and considered inexplicable by Ketelaar (1955). This can be seen in Figure 5 where no obvious difference in the continuum can be detected between the different samples within the measurement uncertainties. Also evident in the figure

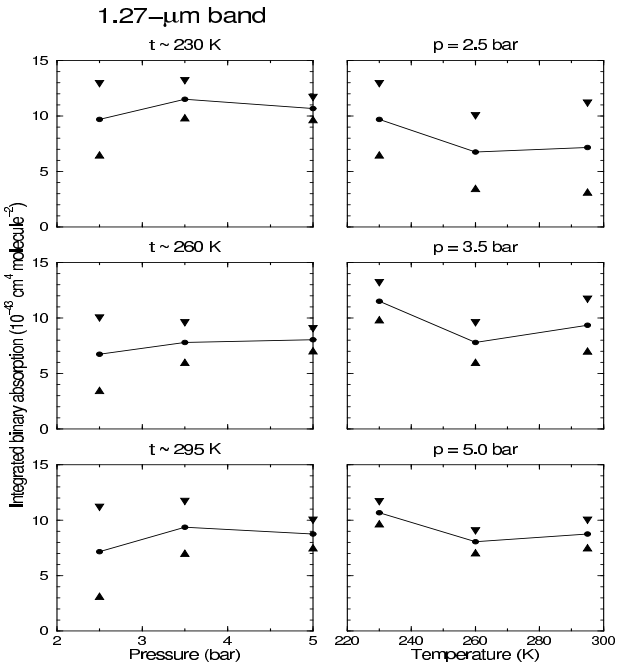

Figure 4. Integrated absorption intensity for the 1.27-μm band. Left column displays variation with pressure keeping temperature constant. Right column displays variation with temperature keeping pressure constant. Triangles mark one standard deviation above and below the resulting integrated absorption calculated by Eq (6).

is the large noise in the spectra for oxygen mixtures, as distinct from the case of pure oxygen.

Assuming that the cross-sections for that band are not changed by the presence of a different gas, as indicated by Figure 5, the results for pure oxygen are more reliable. Averaging the results of nine observations of pure oxygen (numbers 20 to 29, except 25, in Table 2) results in $3.14(\pm 0.97) \times 10^{-43} \mathrm{cm}^4 \mathrm{molecule}^{-2}$ for the integrated binary intensity for the band. The uncertainty is still large but now it is possible to make better comparison with results from other studies. This integrated intensity is used in the calculations in Section 3.

Values for the peak binary absorption cross-section and for the integrated binary intensity from previous studies and for this work are shown in Table 4. The peak absorption of Greenblatt *et al.* (1990) is reported in their paper but the integrated binary intensity was obtained here from the absorption spectrum of pure oxygen at 55 atm and 296 K provided by James Burkholder (personal communication), which was converted to binary cross-section and then integrated. Values of Mlawer *et al.* (1998) were taken directly from their paper except the error in the integrated binary intensity which was estimated from the reported error in the band intensity. The figures attributed to Smith and Newnham (2000) are an average from reported values for mixtures of oxygen and nitrogen at different proportions and temperatures. The values obtained here for the new measurements represent an average made only for the experiments with pure oxygen in order to avoid the huge uncertainties attached to the measurements with mixtures. It is possible to see that the results obtained with those new measurements show an overall

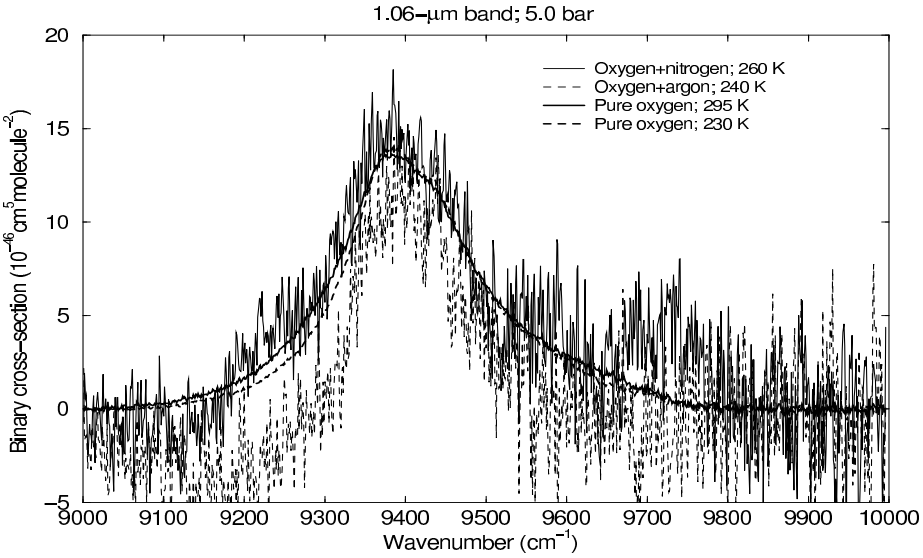

Figure 5. Binary cross-sections of the oxygen 1.06-μm collision-induced band for laboratory measurements at 5.0 bar and different temperatures. All mixtures are 21% oxygen in volume.

agreement with previous studies but the large errors associated with them prevent any conclusive comment. The main reason for the low value of the integrated binary intensity in Mlawer *et al.* (1998) is their choice of a low value for the full width at half maximum (around 135 cm^{-1}0 because of the difficulty of separating out the background in their measurements. Our new measurements point to a considerably large value of about 160 cm^{-1} for the full width at half maximum. Values from Greenblatt *et al.* (1990) are even bigger (240 cm^{-1}).

TABLE 4. PEAK BINARY CROSS-SECTIONS AND INTEGRATED BINARY INTENSITY FOR THE 1.06-μm OXYGEN COLLISION-INDUCED ABSORPTION BAND ACCORDING TO DIFFERENT STUDIES.

	Peak absorption (10^{-46}cm^{5}molecule^{-2})	Integrated binary intensity (10^{-43}cm^{4}molecule^{-2})
Greenblatt *et al.* (1990)	12(±1)	3.5
Mlawer *et al.* (1998)	13.8	2.4(±0.5)
Smith & Newnham (2000)	14.61(±0.46)	2.61(±0.17)
This work	14(±1)	3.14(±0.97)

Integrated binary intensity for Greenblatt *et. al* calculated here from spectrum provided by J. Burkholder (personal communication). Peak absorption and integrated binary intensity for Smith and Newnham are mean values for different oxygen-nitrogen mixtures at different temperatures. Values for this work are an average of different pure oxygen measurements.

2 *1.27-μm collision-induced band*

For this band the collision of oxygen with other gases also contributes to the collision-induced absorption. This is clearly seen in Figure 6, which shows the 1.27-μm-band binary cross-sections for different experiments at 5.0 bar pressure (experiments 5, 9, 12, 18, 24 and 29 in Table 2). The integrated binary intensities for oxygen-nitrogen mixtures experiments (5, 9 and 12), already shown in Table 3, are respectively

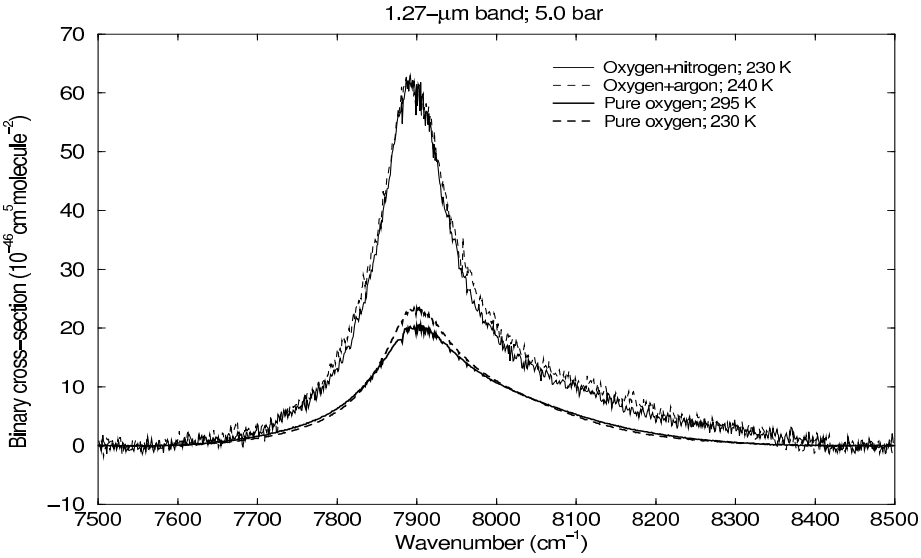

Figure 6. Binary cross-sections of the oxygen 1.27-μm collision-induced band for laboratory measurements at 5.0 bar and different temperatures. All mixtures are 21% oxygen in volume.

$8.75(\pm 1.25)$, $8.04(\pm 1.00)$ and $10.66(\pm 1.00) \times 10^{-43}$cm^{4}molecule^{-2}. For the oxygen-argon mixture and pure oxygen experiments (18, 24 and 29), they are respectively $11.40(\pm 2.63)$, $4.57(\pm 0.13)$ and $4.66(\pm 0.10) \times 10^{-43}$cm^{4}molecule^{-2}. Using the mean integrated intensity values of pure oxygen and oxygen-nitrogen spectra for these 5.0 bar cases resulted in an efficiency factor of 0.26 for nitrogen as a collision partner if compared to oxygen itself (see Appendix). This in reasonable agreement with the value of 0.3 reported by Ketelaar (1955) and Badger *et al.* (1965) and somewhat higher than the value of 0.2 adopted by Zender (1999). It can also be observed that the efficiency of argon molecules as a collision partner is about the same as nitrogen's considering the uncertainties in the present data.

Averaging the integrated binary intensities (and standard deviations) for the nine selected oxygen-nitrogen mixture cases in Table 3 results in a mean binary intensity of $8.85(\pm 2.17) \times 10^{-43}$cm^{4}molecule^{-2} for the 1.27-μm band. This mean value was used in the atmospheric calculations described below.

Averaging the values of Maté *et al.* (1999) for oxygen-nitrogen mixtures at 296, 273, and 253 K results in an integrated intensity of $8.47(\pm 0.13) \times 10^{-43}$cm^{4}molecule^{-2}. In order to obtain a value for comparison from Smith and Newnham (2000), results for 21% oxygen in nitrogen at 200 and 230 K were selected. The monomer integrated intensities were converted to binary units and then added to the dimer integrated binary intensities. The resulting mean value was $12.71(\pm 2.23) \times 10^{-43}$cm^{4}molecule^{-2}. Comparisons between those results and ours are complicated by two reasons: first, Maté *et al.*'s (1999) results are for temperatures much higher than Smith and Newnham's (2000) and the temperature dependency of the cross-sections is not established; second, the uncertainties are large. Considering that our results represent an average over a wide range of temperatures, it can be said that our value compares well with Maté *et al.* (1999) but are about two thirds of Smith and Newnham's (2000) value. Possibly, the subjective method used by Smith and Newnham (2000) to remove the line-structured absorption

(in contrast to the use of RFM/HITRAN96 derived values here) could lead to an overestimate in their integrated intensity. However, a reduction in our result's uncertainties is needed for better assessment and comparisons.

3. ATMOSPHERIC CALCULATIONS

(*a*) *Radiative transfer code and mean binary cross-sections*

A modified version of the delta-Eddington short-wave radiative transfer code of Slingo and Schrecker's (1982), which includes the 220-band structure present in one of the versions of the Edwards and Slingo's (1996); its solar, Rayleigh, water vapour and ozone coefficients were used for the atmospheric calculations. The modifications allowed the inclusion of the short-wave absorption by water vapour and ozone for clear sky atmospheric profiles. The oxygen collisional bands were included as grey absorption by averaging the cross-sections over the model bands (Table 5). Note that no assumption about the oxygen-nitrogen efficiency for the 1.27-μm band need to be made here, as our measurements are made at the same $O_2 : N_2$ ratio as for atmospheric air. In addition, unlike earlier work, the concentration of O_2-O_2 is not required in these calculations, as it is implicitly included in the binary cross-sections.

TABLE 5. THE BAND STRUCTURE OF THE 220-BAND VERSION OF THE MODIFIED SLINGO AND SCHRECKER'S (1982) CODE OVER THE REGIONS OF THE TWO OXYGEN COLLISIONAL ABSORPTION CONTINUA.

Model no.	Limits (cm^{-1})	band no.	Model no.	Limits (cm^{-1})	band no.
	1.27-μm continuum			*1.06-μm continuum*	
155	7500–7600	1	145	9000–9200	1
154	7600–7700	2	144	9200–9400	2
153	7700–7800	3	143	9400–9600	3
152	7800–7900	4	142	9600–9800	4
151	7900–8000	5	141	9800–10,000	5
150	8000–8200	6			
149	8200–8400	7			
148	8400–9600	8			

"Model no." refers to the band numbering inside the model and "band no." is an auxiliary numbering used in this work for each continuum region.

The binary cross-section spectra from each of the nine experiments marked in Table 3 were averaged over the model bands described in Table 5 and then the average amongst the nine resulting figures was performed for each model band.

(*b*) *Effects on a typical atmosphere*

A survey control run with the radiative transfer code was carried out for the McClatchey *et al.* (1972) mid-latitude summer atmospheric profile, solar zenith angle of 60°, surface albedo of 0.1 and total incoming solar irradiance of 1368 Wm^{-2}. Three other runs were performed with the collision-induced absorption by oxygen, two including separately the impact of each continuum and one including both. Figure 7 compares the resulting solar heating rate profiles when no collision-induced absorption is included and when both continua are included. The heating rates in the lower troposphere are increased by about 2%.

When only ozone and water vapour were considered the total short-wave absorbed by the atmosphere was 133.55 Wm^{-2}. When the 1.27-μm continuum only was included the total absorption was 134.35 Wm^{-2} (an increase of 0.80 Wm^{-2} or 0.60% of the total absorbed). When the 1.06-μm continuum only was included, the total absorption was

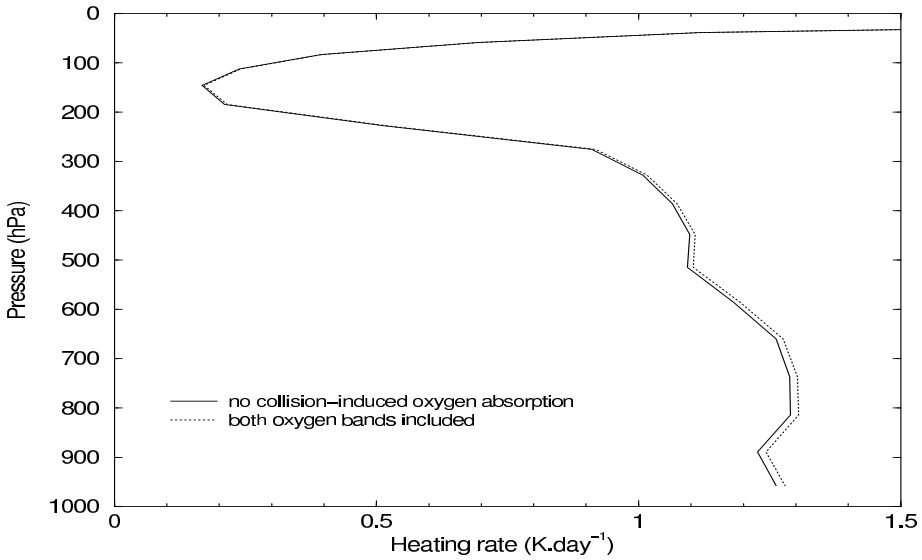

Figure 7. Atmospheric heating rate due to short-wave absorption by ozone and water vapour for a clear-sky mid-latitude summer atmosphere, solar zenith angle 60°, surface albedo 0.1 and total solar irradiance 1368 Wm^{-2}. The near-infrared collision-induced absorption by oxygen is included in one case.

133.85 Wm^{-2} (an increase of 0.30 Wm^{-2} or 0.22% of the total absorbed). Including both bands resulted in 134.65 Wm^{-2} absorbed (1.10 Wm^{-2} or 0.82% increase).

(*c*) *Impact on clear-sky climatological absorbed irradiance*

Monthly zonal means of observed climatological atmospheric profiles of temperature, humidity and ozone averaged over 10-degree-wide latitude belts (see Christidis *et al.* 1997) were used as input to the radiative transfer code in three different situations:

(1) no collision-induced absorption, the control situation,

(2) 1.27-μm band only and

(3) both bands included.

The spatial and temporal variation of the differences (in Wm^{-2}) between (2) and (1) and between (3) and (1) (the impacts of 1.27-μm continuum alone and of both continua together on the atmospheric absorption of solar irradiance) are displayed in Figure 8. The area-averaged (global mean) figures for each situation and differences from control for the mid-season months are in Table 6. Also in same table the average of the area-averaged values for the four months (taken as the annual mean). Note that most of the earlier studies of the impact of the collision-induced absorption used rather crude techniques to derive a global-mean from a single profile. The exception is Zender (1999) who included the absorption within a GCM radiation scheme and used the GCM to produce a better seasonal and global average. A disadvantage with his technique is that the GCM radiation radiation code is comparatively wide (it represents the near-infrared absorption by water vapour in 7 k-distribution bins). This prevented a separation of the impact of the 1.06-μm and 1.27-μm bands.

As the column amount of oxygen is almost constant with latitude (having some small variation influenced by orography), the main modulator of the collision-induced absorption is the solar irradiance available in the atmospheric column. Because of that

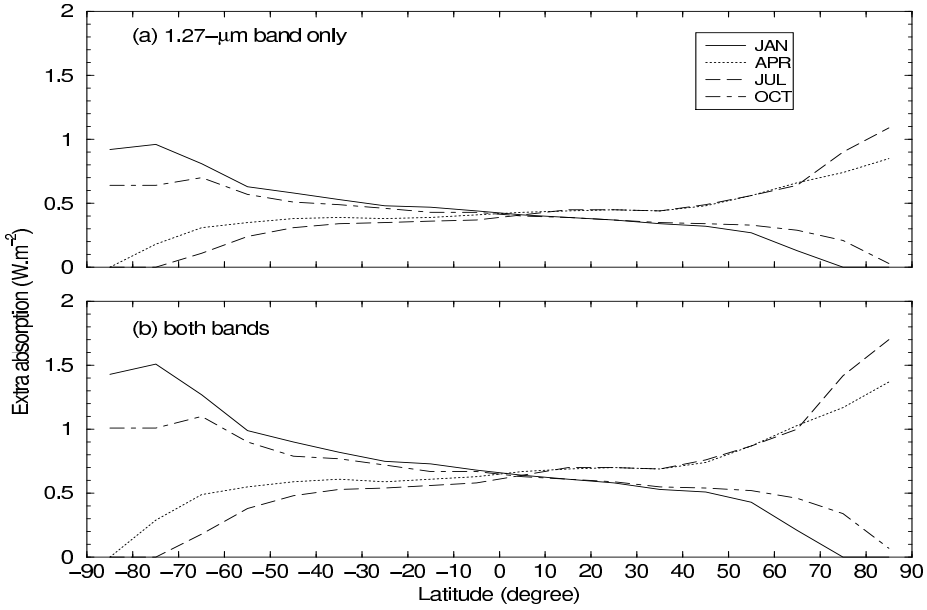

Figure 8. Impact on the solar irradiance absorbed by atmospheric ozone and water vapour for mid-season monthly climatological conditions averaged over 10-degree-latitude belts when (a) the 1.27-μm collision-induced absorption band of oxygen and (b) the 1.27-μm and 1.06-μm bands are included (estimates for clear skies).

TABLE 6. MID-SEASON AND ANNUAL GLOBAL AVERAGES OF ABSORBED SOLAR RADIATION (IN Wm^{-2}).

	January	April	July	October	average
(1) Control	63.20	62.13	61.74	62.27	62.09
(2) 1.27-μm only	63.64	62.56	62.14	62.68	62.51
(3) Both bands	63.81	62.70	62.30	62.86	62.67
(2) – (1)	0.44	0.43	0.40	0.41	0.42
(3) – (1)	0.61	0.57	0.56	0.59	0.58

(1) Water vapour and ozone only; (2) 1.27-μm collision-induced band added; (3) 1.27-μm and 1.06-μm bands added; last two rows are differences representing the absorption due to the collision-induced bands only.

the maxima of extra absorption are near the South Pole in October and January and near the North Pole in April and July. At these times and locations, the collision-induced absorption contributes 3–4% of the total due to water vapour and ozone. This latitudinal variation is in contrast to that due to variations in water vapour spectral line parameters, that falls off heavily with latitudes (Chagas *et al.* 2001).

4. CONCLUSIONS

The earlier estimates of atmospheric absorption by these continua were summarised in Table 1. The differences amongst the various estimates are mainly due to the lack of good-quality high-resolution cross-sections for the collisional bands, especially for the relatively strongly absorbing 1.27-μm band. For the 1.06-μm band, most of these studies used the cross-sections of Greenblatt *et al.* (1990). For the 1.27-μm band some crude estimates were in general used. Maté *et al.* (1999) presented cross-sections for

the 1.27-μm band from measurements with pure oxygen and oxygen-nitrogen mixtures at different conditions. Smith and Newnham (1999, 2000) also reported high-resolution cross-sections for oxygen-nitrogen mixtures at different conditions. To our knowledge, those recent measurements were not used to estimate the global impact on atmospheric absorption.

Here we describe new measurements of the 1.06-μm and 1.27-μm oxygen collision-induced absorption bands and their use to estimate the global impact of oxygen collision-induced absorption on atmospheric absorption. Cross-sections derived from measurements on "air" (21% oxygen in nitrogen) samples were used when the noise was not too large. No pressure or temperature dependence of the integrated binary intensities could be detected.

Cross-sections from nine experiments were averaged over the appropriate bands of a 220-band radiative transfer model modified from the Slingo and Schrecker's (1982) code to calculate clear-sky atmospheric absorption from water vapour and ozone using parameters from Edwards and Slingo (1996). The data spread for the 1.27-μm band was smaller than for the 1.06-μm one. Calculations for a mid-latitude summer atmosphere resulted in 0.82% extra absorption for the two oxygen collision bands (0.60% due to the 1.27-μm band and 0.22% due to the 1.06-μm band).

Estimates for 10-degree-latitude-belt monthly climatological atmospheric profiles made possible the assessment of the latitudinal and seasonal variation of the impacts. Being mostly modulated by the solar radiation available to the atmosphere (oxygen column amount has a very small spatial variation), globally averaged impacts are larger in January (smaller Earth-Sun distance) and smaller in July. The maxima of absorption are near the South Pole in October and January and near the North Pole on April and July. Global and annual mean were 0.58 Wm^{-2} for the two band considered. Adding 0.42 Wm^{-2} for the visible band (based on Greenblatt *et al.* 1990) and 0.03 Wm^{-2} for the 1.58-μm band (Mlawer *et al.* 1998) leads to an estimate of 1.03 Wm^{-2} global annually averaged impact. This is a significant (1.7%) increase on top of the 62.1 Wm^{-2} mean absorption by water vapour and ozone and even more significant in relation to the figure of 10–20 Wm^{-2} of the "unexplained" atmospheric short-wave absorption cited by some authors. The dominant uncertainty is in the 1.27-μm integrated cross-sections (roughly 25%); our estimates of the increase in absorption are accordingly uncertain by 25%.

Apart from the confirmation of other studies' conclusions that the collision-induced absorption by oxygen is not negligible in the atmosphere, an important conclusion of this study is that high-resolution measurements using long pathlengths under controlled conditions in the laboratory are still needed to complement the high-pressure shorter pathlength observations reported here. In particular future measurements should better characterize the temperature dependence of the 1.06-μm collision-induced absorption region.

ACKNOWLEDGEMENTS

J. C. S. Chagas acknowledges funding from CAPES, Ministry of Education, Brazil (Process BEX0928/96-8); Anu Dudhia is thanked for his help in using RFM; The Natural Environment Research Council is thanked for the provision of time on the Molecular Spectroscoopy Facility at the Rutherford Appleton Laboratory. J. Burkholder (NOAA Aeronomy Laboratory) is thanked for providing the digital data from Greenblatt *et al.* (1990).

APPENDIX

Nitrogen efficiency

In order to estimate the efficiency ϵ of nitrogen (or other gaseous species) as a collision partner if compared to oxygen itself, we start with an idealised situation 1 where the integrated binary cross-section S_1 (see Eq (6)) for a sample of N molecules of pure oxygen is evaluated:

$$S_1 = S_{O_2}, \tag{A.1}$$

where S_{O_2} is the binary cross-section due to oxygen-oxygen collisions.

Another situation is then achieved by adding $3.76N$ molecules of nitrogen to the original pure oxygen sample. This particular value (3.76) was used here in order to obtain a resulting sample with 21% oxygen ($N/4.76N$) in 79% nitrogen ($3.76N/4.76N$) but could have been easily generalised. The resulting integrated binary cross-section for situation 2 would be:

$$S_2 = S_{O_2} + S_{N_2}, \tag{A.2}$$

where S_{N_2} is the binary cross-section due to nitrogen-oxygen collisions. Eq (A.2) can be rewritten as:

$$S_2 = S_{O_2} + \epsilon \times 3.76 S_{O_2}. \tag{A.3}$$

If nitrogen is totally "inefficient" ($\epsilon = 0$) as a collision partner (as in the case of the 1.06-μm collision-induced band), S_{N_2} would be zero and $S_2 = S_{O_2} = S_1$. If nitrogen is as efficient as oxygen ($\epsilon = 1$) in producing collision-induced absorption, S_{N_2} would be 3.76 times bigger than S_{O_2} because the number of nitrogen molecules in the sample is 3.76 times the number of oxygen molecules. In this case, $S_2 = S_{O_2} + 3.76 S_{O_2}$ or $S_2 - S_1 = 3.76 S_1$.

The unknown efficiency factor ϵ can be calculated using:

$$S_2 - S_1 = \epsilon \times 3.76 S_1, \text{ or} \tag{A.4}$$

$$\epsilon = \frac{S_2 - S_1}{3.76 S_1}. \tag{A.5}$$

In the text (Section 2(e)2), the mean integrated binary cross-section at 5.0 bar pressure is $4.62 \times 10^{-43} \mathrm{cm}^4 \mathrm{molecule}^{-2}$ for the pure oxygen samples (S_1) and $9.15 \times 10^{-43} \mathrm{cm}^4 \mathrm{molecule}^{-2}$ for the 21% oxygen in nitrogen mixtures (S_2). Using these values in Eq (A.5) results in $\epsilon = 0.26$.

REFERENCES

Arking, A. 1999a Bringing climate models into agreement with observations of atmospheric absorption. *J. Climate*, **12,** 1589–1600

Arking, A. 1999b The influence of clouds and water vapor on atmospheric absorption. *Geophys. Res. Lett.*, **26,** 2729–2732

Brown, P. D., Clough, S. A., Mlawer, E. J., Shippert, T. R. and Murcray, F. J. 1999a High resolution validation in the shortwave: ASTI/LBLRTM QME. *Proc. Eighth ARM Science Team Meeting*, DOE/ER-0738, US DOE, 101–108

Brown, P. D., Mlawer, E. J., Clough, S. A., Murcray, F. J., Dybdahl, A. W., Shippert, T. R., Harrison, L. C., Kiedron, P. W. and Michalsky, J. J. 1999b High-resolution model/measurement validations of solar direct-beam flux. *Proc. Ninth ARM Science Team Meeting*, US DOE

Badger, R. M., Wright, A. C. and Whitlock, R. F. 1965 Absolute intensities of the discrete and continuous absorption bands of oxygen gas at 1.26 and 1.065 μ and the radiative lifetime of the $^1\Delta_g$ state of oxygen. *J. Chem. Phys.*, **43,** 4345–4350

Chagas, J. C. S., Newnham, D. A., Smith, K. M. and Shine, K. P. 2001 Effects of improvements in near-infrared water vapour line intensities on short-wave atmospheric absorption. *Geophys. Res. Lett.*, **28,** 2401–2404

Cho, C. W., Allin, E. J., and Welsh, H. L. 1963 Effect of high pressures on the infrared and red atmospheric absorption band systems of oxygen. *Can. J. Phys.*, **41,** 1991–2002

Christidis, N., Hurley, M. D., Pinnock, S., Shine, K. P. and Wallington, T. J. 1997 Radiative forcing of climate change by CFC-11 and possible CFC replacements. *J. Geophys. Res.*, **102,** 19597–19609

Cusack, S., Slingo, A., Edwards, J. M. and Wild, M. 1998 The radiative impact of a simple aerosol climatology on the Hadley Centre atmospheric GCM. *Q. J. R. Meteorol. Soc.*, **124,** 2517–2526

Dianov-Klokov, V. I. 1964 Absorption spectrum of oxygen at pressures from 2 to 35 atm in the region from 12,600 to 3600 A. *Opt. Spectros., Engl. Transl.*, **16,** 224–227

Dudhia, A. 1997 *RFM v3 software user's manual*, ESA Document PO-MA-OXF-GS-003, Dept. of Atmospheric, Oceanic and Planetary Physics, University of Oxford

Edwards, J. M., and Slingo, A. 1996 Studies with a flexible new radiation code. I: Choosing a configuration for a large-scale model. *Q. J. R. Meteorol. Soc.*, **122,** 689–719

Greenblatt, G. D., Orlando, J. J., Burkholder, J. B. and Ravishankara, A. R. 1990 Absorption measurements of oxygen between 330 and 1140 nm. *J. Geophys. Res.*, **95,** 18557–18582

Halthore, R. N. and Schwartz, S. E. 2000 Comparison of model-estimated and measured diffuse downward irradiance at surface in cloud-free skies. *J. Geophys. Res.*, **105,** 20165–20177

Kato, S., Ackerman, T. P., Clothiaux, E. E., Mather, J. H., Mace, G. G., Wesely, M. L., Murcray, F. and Michalsky, J. 1997 Uncertainties in modelled and measured clear-sky surface shortwave irradiances. *J. Geophys. Res.*, **102,** 25881–25898

Ketelaar, J. A. A. 1955 La trasition triplet-singlet dans l'oxygene sous pression. *Nuovo Cimento*, **II,** suppl., ser X, 3, 763–765

Maté, B., Lugez, C., Fraser, G. T. and Lafferty, W. J. 1999 Absolute intensities for the O_2 1.27 μm continuum absorption. *J. Geophys. Res.*, **104,** 30585–30590

McClatchey, R. A., Volz, F. E., Fenn, R. W., Garing, J. S. and Selby, J. E. A. 1972 *Optical properties of the atmosphere.* Air Force Cambridge Research Laboratory, AFCRL–72–0497

McKellar, A. R. W., Rich, N. R. and Welsh, H. L. 1972 Collision-induced vibrational and electronic spectra of gaseous oxygen at low temperatures. *Can. J. Phys.*, **50,** 1–9

Mlawer, E. J., Clough, S. A., Brown, P. D., Stephen, T. M., Landry, J. C., Goldman, A. and Murcray, F. 1998 Observed atmospheric collision-induced absorption in near-infrared oxygen bands. *J. Geophys. Res.*, **103,** 3859–3863

Newnham, D. A., and Ballard, J. 1998 Visible absorption cross sections and integrated absorption intensities of molecular oxygen (O_2 and O_4). *J. Geophys. Res.*, **103,** 28801–28816

Osterkamp, H., Ferlemann, F., Harder, H., Perner, D., Platt, U., Schneider, M. and Pfeilsticker, K. 1998 First measurement of the atmospheric O_4 profile. In: Proceedings of the Fourth European Symposium on Polar Stratospheric Ozone, *Air Pollut. Res. Rep.* **66,** 478–481

Pfeilsticker, K., Erle, F. and Platt, U. 1997 Absorption of solar radiation by atmospheric O_4. *J. Atm. Sci.*, **54,** 933–939

Rothman, L. S., Rinsland, C. P., Goldman, A., Massie, S. T., Edwards, D. P., Flaud, J.-M., Perrin, A., Camy-Peyret, C., Dana, V., Mandin, J.-Y., Schroeder, J., McCann, A., Gamache, R. R., Watson, R. B., Yoshino, K., Chance, K. V., Jucks, K. W., Brown, L. R., Nemtchinov, V. and Varanasi P.	1998	The HITRAN molecular spectroscopic database and HAWKS (HITRAN Atmospheric Workstation): 1996 edition. *J. Quant. Spectrosc. Radiat. Transfer*, **60,** 665–710
Slingo, A., and Schrecker, H. M.	1982	On the shortwave radiative properties of stratiform water clouds. *Q. J. R. Meteorol. Soc.*, **108,** 407–426
Smith, K. M., and Newnham, D. A.	1999	Near-infrared absorption spectroscopy of oxygen and nitrogen gas mixtures. *Chem. Phys. Lett.*, **308,** 1–6
Smith, K. M., and Newnham, D. A.	2000	Near-infrared absorption cross-sections and integrated absorption intensities of molecular oxygen (O_2, O_2-O_2, and O_2-N_2). *J. Geophys. Res.*, **105,** 7383–7396
Solomon, S., Portmann, R. W., Sanders, R. W. and Daniel, J. S.	1998	Absorption of solar radiation by water vapour, oxygen, and related collision pairs in the earth's atmosphere. *J. Geophys. Res.*, **103,** 3847–3858
Vaida, V., Daniel, J. S., Kjaergaard, H. G., Goss, L. M. and Tuck, A. F.	2001	Atmospheric absorption of near infrared and visible solar radiation by the hydrogen bonded water dimer. *Q. J. R. Meteorol. Soc.*, **127,** 1627–1643
Vigasin, A. A.	1996	On the nature of collison-induced absorption in gaseous homonuclear diatomics. *J. Quant. Spectrosc. Radiat. Trans.*, **56,** 409–422
Wild, M.	1999	Discrepancies between model-calculated and observed shortwave atmospheric absorption in areas with high aerosol loadings. *J. Geophys. Res.*, **104,** 27361–27371
Wild, M., and Ohmura, A.	1999	The role of clouds and the cloud-free atmosphere in the problem of underestimated absorption of solar radiation in GCM atmospheres. *Phys. Chem. Earth(B)*, **24,** 261–268
Zender, C. S.	1999	Global climatology of abundance and solar absorption of oxygen collision complexes. *J. Geophys. Res.*, **104,** 24471–24484
Zender, C. S., Bush, B., Pope, S. K., Bucholtz, A., Collins, W. D., Kiehl, J. T., Valero, F. P. J. and Vitko Jr., J.	1997	Atmospheric absorption during the Atmospheric Radiation Measurement (ARM) Enhanced Shortwave Experiment (ARESE). *J. Geophys. Res.*, **102,** 29901–29915
Zhong, W., Haigh, J. D., Belmiloud, D., Schermaul, R. and Tennyson, J.	2001	The impact of new water vapour spectral line parameters on the calculation of atmospheric absorption (8600–15000 cm^{-1}). *Q. J. R. Meteorol. Soc.*, **127,** 1615–1626